Published version available at: https://doi.org/10.1016/j.combustflame.2017.04.019

Controlling of flame propagation in a composite solid energetic material: from stabilization to chaotic regimes

Vadim N. Kurdyumov [a], Vladimir V. Gubernov [b,d], Roman V. Fursenko [c,d]

[a] *Department of Energy, CIEMAT, Avda. Complutense 40, 28040 Madrid, Spain*
[b] *P.N.Lebedev Physical Institute, 53 Leninsky pr., Moscow, 119991 Russia*
[c] *Institute of Theoretical and Applied Mechanics, Novosibirsk, 630090, Russia*
[d] *Far Eastern Federal University, 8 Suhanova St., Vladivostok 690950, Russia*

Abstract

The flame propagation in a solid composite energetic sample comprised of a solid energetic annulus surrounding a highly conductive core is investigated using one-step Arrhenius reaction mechanism. The steady-state solutions, its linear stability analysis and the results of direct numerical simulations of non-stationary problem are presented. It was found that the flame dynamics is highly subject to variation in the presence of the conductive core leading in some cases to a chaotic flame behavior or to stabilization of the flame propagation. It was demonstrated that for given combustion properties of the energetic material the kind of flame dynamics observed in the composite sample can be controlled by an appropriate choice of the experimental parameters such as the thickness of the fuel annulus deposited or the diameter of the heat conductive core.

1 Introduction

The onset of pulsations quite often accompanies the propagation of combustion waves in solid combustion fuels. One of the first experimental observation was reported in [1]. In the latter experimental papers [2, 3] it was demonstrated that pulsations are of auto-oscillatory nature and that complex temporal regimes can emerge as the bifurcation parameters (mixture dilution) are modified. Besides planar one-dimensional oscillations in cylindrical solid fuel samples multidimensional regimes of flame propagation such as spinning waves were found while conducting the self-propagating high temperature synthesis [4, 5]. More detailed description of the variety of spatio-temporal wave patterns observed in combustion of solid fuels can be found in reviews [6–8].

Systematic mathematical analysis of oscillatory flame propagation regimes began with the publication of the results in [9], where it was demonstrated by means of numerical modeling that the planar flame pulsations are of diffusional-thermal nature and can be described within the models which take into consideration heat release occurring in course of fuel consumption and heat diffusion from hot products to the fresh mixture. Further advances in the analysis of flame pulsations came from the employment of the asymptotic analysis [10]. It was demonstrated that the planar combustion wave loses stability due to the Hopf bifurcation and the critical parameter values for the onset of oscillations and characteristics of these oscillating regimes were determined. These findings were later confirmed in numerical analysis in [11, 12].

In the case of the cylindrical geometry it was shown [13] that as the diameter of the sample is increased either traveling or one-dimensional pulsating instabilities occur, which can result in the emergence of spinning or pulsating regimes of combustion wave propagation. The results of the stability and bifurcation asymptotic analysis in the limit of the large activation energy are summarized in [14]. Extensive numerical results of combustion wave propagation in cylindrical samples were presented in [15–19] where the emergence of different nonstationary and/or multidimensional regimes of flame propagation was reported. In [20] the numerical stability analysis of combustion wave propagation in cylindrical fuel sample was undertaken and the formation of different modes of spinning waves was directly related with the global stability characteristics of two-dimensional traveling wave solutions.

Initiated by the works in [21, 22] the idea to develop the solid nanostructured composite energetic materials is actively discussed. These materials structurally are comprised of the solid fuel shell which provides the heat due to the chemical reaction and inert core with high thermal conductivity, which serves as a thermal conduit to recuperate heat from hot products of the reaction to the fresh fuel mixture. The core can be made of carbon nanotubes [22], metal/metal-oxide nanowires [23] or carbon fibers [24], while standard energetic materials such as nitrocellulose are used in shell of the composite.

In [25, 26] we have employed a one-dimensional model in order to investigate the properties of combustion waves in such systems. The flame speed enhancement is estimated by using asymptotic and numerical analysis and it is demonstrated that the optimal design of composite material can result in significant stabilization of combustion waves. The aim of this work is to extend our previous analysis to investigate the complex dynamical regimes, which emerge as the traveling combustion wave becomes unstable with respect to flame oscillations. To this end, in Section 2 we give the general formulation and asymptotic assumptions used in the study;

the numerical treatment is briefly described in Section 3; the numerical results describing the steady-state traveling wave solutions are presented in Section 4; the linear stability analysis formulation is given in Section 5; the linear stability results are presented in Section 6; the results of direct numerical calculations are given in Section 7, with the results of calculations of the Lyapunov characteristic exponent in Section 8. Finally, conclusions are drawn in the last section.

2 General formulation

Consider an annulus of energetic material capable of exothermic decomposition surrounding a thin cylinder of high thermal conductivity (e.g. a carbon nanotube), both mediums are at initial temperature T_0. A sketch of the geometry is shown in Fig. 1. In what follows we assume that the heat capacities, c_1 and c_2, the heat conductivities, λ_1 and λ_2, and the densities, ρ_1 and ρ_2, are all constant, where indexes 1 and 2 correspond to the energetic annulus and the core, respectively. We suppose that the heat losses from the outer surface of the sample are negligible while the heat exchange between the annulus and the core obeys a linear law, $q = K(T_1 - T_2)$, where q is the heat flux through the surface separating the core and the annulus, per unit area, and K is an effective heat-exchange coefficient. Following [25, 26] we assume that the temperature of the shell and core can be effectively averaged across the corresponding regions, namely both temperatures are functions of x and t only. The heat-exchange coefficient K can be calculated, for example, supposing that the core and the annulus are separated by a thin membrane. Then, $K = \lambda_w/h_w$, where λ_w and h_w are the mambrane conductivity and its thickness, respectively.

The combustion process is modeled by an irreversible reaction of the form $F \to P + Q$, where F denotes the combustible substance, P is the product, and Q is the heat released per unit mass of fuel. The combustion rate, Ω, defined as the mass of fuel consumed per unit volume and unit time, is assumed to follow an Arrhenius law of the form

$$\Omega = \rho_1 \mathcal{B} Y \exp(-E/\mathcal{R}T_1),$$

where $\mathcal{B}$, Y, E and $\mathcal{R}$ represent, respectively, the pre-exponential factor, the mass fraction of combustible substance, the activation energy and the universal gas constant.

In order to describe the flame propagation a reference frame attached to the flame is used. Following the temperature distribution along the energetic material, $T_1(x, t)$, starting from the unburned side, we choose a point $x = x_*$ (the first point if there are more than one) where

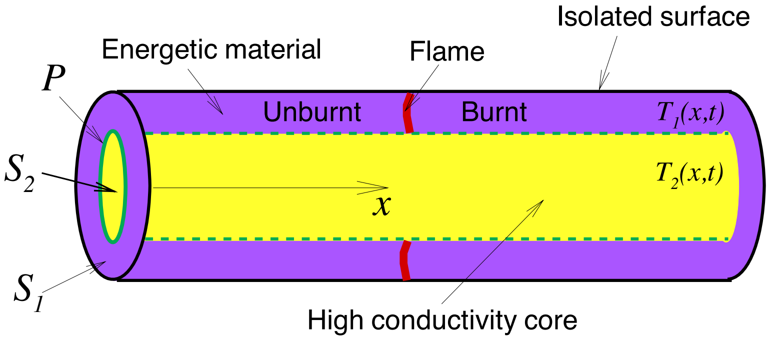

Figure 1: Sketch of the problem

the temperature is equal to some value $T_1 = T_*$ (the reference temperature below). In the following, the reference frame is attached to this point. In the case of steady flame propagation it moves as an invariable structure with a constant velocity equal to U_f independent on T_*. In the general case the velocity U_f of this point as a function of time characterizes the time-dependent development of the combustion process. The value of U_f is determined by the condition

$$T_1(x_*, t) = T_* \tag{1}$$

Evidently, T_* must be chosen judiciously, less than the maximum temperature seen during the process, and greater than the minimum temperature T_0. For the unsteady flame dynamics, the flame does not move as an intact structure and the specific form of U_f depends on the choice of the reference temperature T_*. Anticipating the numerical results presented below the level of randomness (the Lyapunov characteristic exponent) becomes affected by the choice of T_* in the cases of stochastically propagating flames.

Under above simplifications, the dimensional balance equations describing conservations of mass of fuel and energy in both mediums take the form

$$S_1\left\{\rho_1\frac{\partial Y}{\partial t} + \rho_1 U_f\frac{\partial Y}{\partial x} - \Omega\right\} = 0, \tag{2}$$

$$S_1\left\{\rho_1 c_1\frac{\partial T_1}{\partial t} + \rho_1 c_1 U_f\frac{\partial T_1}{\partial x} - \lambda_1\frac{\partial^2 T_1}{\partial x^2} - Q\Omega\right\} = -PK(T_1 - T_2), \tag{3}$$

$$S_2\left\{\rho_2 c_2\frac{\partial T_2}{\partial t} + \rho_2 c_2 U_f\frac{\partial T_2}{\partial x} - \lambda_2\frac{\partial^2 T_2}{\partial x^2}\right\} = PK(T_1 - T_2), \tag{4}$$

where S_1, S_2 are the areas of the solid combustible and pure conductive sections, respectively, and P is the perimeter of the intermediate surface.

The mass fraction is normalized below with respect to its upstream value, Y_0, and non-dimensional temperatures $\theta_1 = (T_1 - T_0)/(T_a - T_0)$ and $\theta_2 = (T_2 - T_0)/(T_a - T_0)$ are based on the adiabatic flame temperature $T_a = T_0 + QY_0/c_1$ corresponding to a planar flame propagation in the pure energetic material. Let us define the characteristic time and length using the relations

$$t_c = \beta \mathcal{B}^{-1} \exp(E/\mathcal{R}T_a), \quad l_c = \sqrt{t_c \alpha_1}, \tag{5}$$

where $\beta = \gamma E/RT_a$ is the Zel'dovich number and $\gamma = (T_a - T_0)/T_a$ is the heat release parameter. The non-dimensional governing equations take the form

$$\frac{\partial Y}{\partial t} + u_f \frac{\partial Y}{\partial x} = -\omega. \tag{6}$$

$$\frac{\partial \theta_1}{\partial t} + u_f \frac{\partial \theta_1}{\partial x} = \frac{\partial^2 \theta_1}{\partial x^2} + \omega - \xi \cdot (\theta_1 - \theta_2), \tag{7}$$

$$\frac{\partial \theta_2}{\partial t} + u_f \frac{\partial \theta_2}{\partial x} = \alpha \frac{\partial^2 \theta_2}{\partial x^2} + s \cdot \xi \cdot (\theta_1 - \theta_2), \tag{8}$$

The parameters appearing in the above equations are

$$\xi = \frac{KP\beta \exp(E/RT_a)}{\rho_1 c_1 S_1 \mathcal{B}}, \quad \alpha = \frac{\alpha_2}{\alpha_1}, \quad s = \frac{\rho_1 c_1 S_1}{\rho_2 c_2 S_2}, \tag{9}$$

where $\alpha_1 = \lambda_1/\rho_1 c_1$ and $\alpha_2 = \lambda_2/\rho_2 c_2$ are the thermal diffusivities. It is noteworthy that the parameter s can be easily changed in experiments by varying the cross-section of the conductive core or deposited mass of the energetic material in the annulus. In the limit $\xi \to 0$ Eqs. (6)-(7) become identical to those describing a standard one-dimensional combustion wave propagating in the pure energetic sample [9].

In the following we assume that that the cross-section of the conductive core is small compared with that of the solid combustible, $S_2 \ll S_1$, and, simultaneously, it has a very high thermal conductivity compared with that of the energetic annulus, namely $\lambda_2 \gg \lambda_1$. In term of the non-dimensional parameters it means that $s \gg 1$ and $\alpha \gg 1$. It is convenient to introduce a parameter μ defined as

$$\mu = \frac{\alpha}{s} = \frac{\lambda_2}{\lambda_1} \cdot \frac{S_2}{S_1}. \tag{10}$$

Always supposing that $\mu = O(1)$, Eq. (8) takes in the limit $s \to \infty$ the following quasi-steady form

$$0 = \mu \frac{\partial^2 \theta_2}{\partial x^2} + \xi \cdot (\theta_1 - \theta_2). \tag{11}$$

This approximation describes conductive cores of negligible heat capacity with non-negligible heat transfer effect. This situation corresponds to an experimental setup where the single carbon nanotube form the heat conducting core of the composite material [22].

The dimensionless reaction rate ω appearing in Eqs. (6)-(7) is given by

$$\omega = \beta Y \exp\left\{\frac{\beta(\theta_1 - 1)}{1 + \gamma(\theta_1 - 1)}\right\} \tag{12}$$

The factor β appearing in Eq. (12) provides that $u_f \to 1$ for the steady combustion wave in the pure energetic material in the limit $\beta \to \infty$.

The instantaneous values of $u_f(t) = t_c U_f / l_c$ are determined by the additional condition

$$\theta_1(x_*, t) = \theta_*, \tag{13}$$

where $\theta_* = (T_* - T_0)/(T_a - T_0)$ is the non-dimensional reference temperature. Evidently, all results should be independent on x_* due to translation invariance along the direction of motion, $x \to x + const$.

Appropriate boundary conditions corresponding the configuration depicted in Fig. 1 are

$$\begin{aligned} x \to -\infty : \quad & \theta_1 = \theta_2 = Y - 1 = 0, \\ x \to +\infty : \quad & \partial Y/\partial x = \partial\theta_1/\partial x = \partial\theta_2/\partial x = 0. \end{aligned} \tag{14}$$

Finally, the problem of the flame propagation in the composite energetic sample is reduced to solve Eqs. (6)-(7) and (11) subject to the boundary conditions given by Eq. (14).

3 Numerical treatment

Steady as well as time-dependent computations were carries out in a finite domains, $x_{min} < x < x_{max}$. The typical values were $x_{min} = -20$ and $x_{max} = 20$. The spatial derivatives were disretized on a uniform grid using second order three-point central differences for the temperature in Eq. (7) and three-point upwind differences for the convection term of Eq. (6). The typical number of grid points was 2001. For time-dependent computations an explicit marching procedure was used in time with the typical time step $\tau = 10^{-4}$. The number of grid points was doubled in some cases and τ was halved without any significant differences in the results. In order to determine steady solutions (but not necessary stable), the steady counterpart $(\partial/\partial t \equiv 0)$ of Eqs. (6)-(7) were solved together with Eq. (11) using a Gauss-Seidel method with over-relaxation.

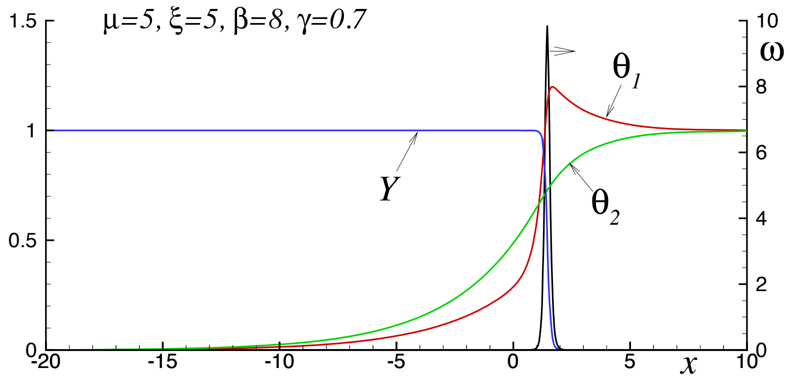

Figure 2: Typical steady mass fraction and temperatures profiles computed using the reduced model given by Eqs. (7), (6) and (11).

4 Steady-state solutions

Consider first the steadily propagating flames imposing $\partial/\partial t = 0$ in Eqs. (6), (7) which were solved together with Eqs. (11) and (14). The system has the first integral,

$$u_f(\theta_1 + Y - 1) = \frac{d\theta_1}{dx} + \mu\frac{d\theta_2}{dx}, \tag{15}$$

indicating, together with Eq. (11), that $\theta_1 \to 1$ and $\theta_2 \to 1$ behind the flame where the fuel mass fraction and temperature gradients approach to zero value.

Figure 2 illustrates the typical distributions of the mass fraction and temperatures plotted for $\mu = 5$, $\xi = 5$, $\beta = 8$ and $\gamma = 0.7$. The distinctive characteristic of the temperature profile in the energetic material is the existence of a local maximum appearing just after the reaction zone with the super-adiabatic temperature, $\theta_{1\,max} > 1$.

The dimensionless steady velocity u_f is shown in Fig. 3 (left plot) together with the temperature maximum, $\theta_{1\,max}$ (right plot), as functions of μ for various ξ, all curves calculated for $\beta = 8$ and $\gamma = 0.7$. It can be seen in Fig. 3 that the temperature in the annulus can be more than 30% higher than the adiabatic flame temperature in pure solid fuel, while the flame speed can increase in more than five times. The figure shows also that for small values of μ the maximum temperature $\theta_{1\,max}$ approaches to unity and the flame velocity becomes $u_f \approx 1.02$ calculated for $\beta = 8$, $\gamma = 0.7$ and $\mu = 0$. It can be explained by the fact that the effect of the conductive core becomes negligible not only for $\xi \to 0$, as it was mentioned above, but also for $\mu \to 0$ when $\theta_1 \approx \theta_2$.

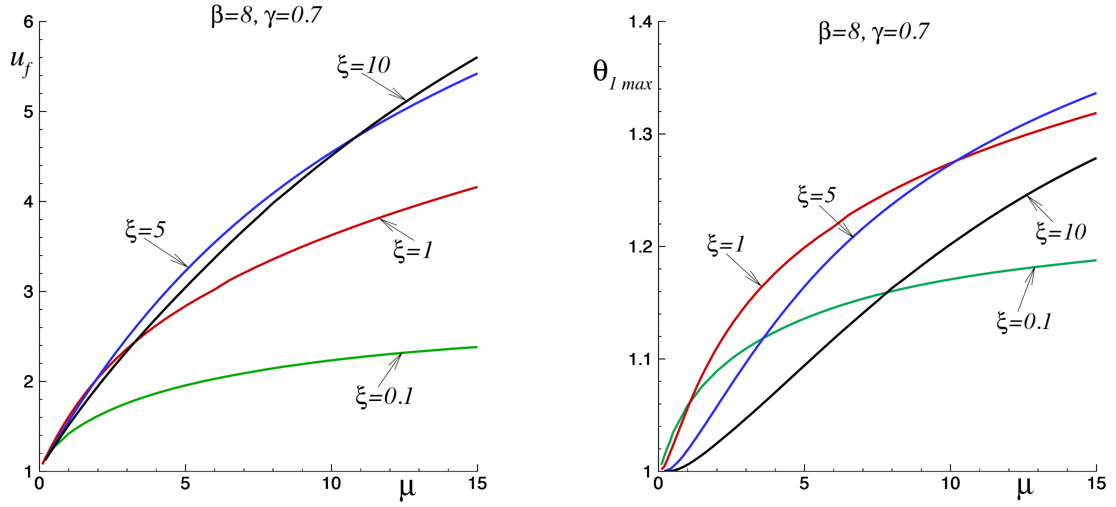

Figure 3: Computed steady flame velocity u_f (left) and maximum of the temperature θ_1 (right) as a function of μ; for $\beta = 8, \gamma = 0.7$ and several values of ξ.

5 Linear stability analysis formulation

Stability analysis of the steady-state flames presented in the previous section has been carried out using the method described in detail in [27]. The distributions of the steady-state temperatures, mass fraction and the flame propagation velocity, all now denoted by subindex "0", are perturbed as usual with small perturbations

$$\begin{aligned} \theta_i &= \theta_{i0}(x) + \epsilon\Phi_i(x)\exp(\lambda t), \quad i = 1, 2, \\ Y &= Y_0(x) + \epsilon\Psi(x)\exp(\lambda t), \\ u_f &= u_{f0} + \epsilon u_{f1}\exp(\lambda t), \end{aligned} \tag{16}$$

where λ is a complex number, the real part of which represents of the growth rate, and ϵ is a small amplitude. The linearized eigenvalue problem obtained when substituting Eqs. (16) into Eqs. (6),(7) and (11) reduces to find non-trivial solutions of the system

$$\lambda\Psi + u_{f1}Y_0^I + u_{f0}\Psi^I = -A\Phi_1 - B\Psi, \tag{17}$$

$$\lambda\Phi_1 + u_{f1}\theta_0^I + u_{f0}\Phi_1^I = \Phi_1^{II} + A\Phi_1 + B\Psi - \xi(\Phi_1 - \Phi_2), \tag{18}$$

$$0 = \mu\Phi_2^{II} + \xi(\Phi_1 - \Phi_2). \tag{19}$$

Here "I" denotes the differentiation with respect to x and

$$A = \frac{\beta^2 Y_0}{[1+\gamma(\theta_{10}-1)]^2} \exp\left\{\frac{\beta(\theta_{10}-1)}{1+\gamma(\theta_{10}-1)}\right\}, \quad B = \beta \exp\left\{\frac{\beta(\theta_{10}-1)}{1+\gamma(\theta_{10}-1)}\right\}$$

are both functions of x. The constraint following from Eq. (13) becomes

$$\Phi_1(x_*) = 0 \tag{20}$$

The solution of Eqs. (17-19) is sought in the form

$$(\Psi, \Phi_1, \Phi_2) = (\Psi_h, \Phi_{1h}, \Phi_{2h}) + c \cdot (dY_0/dx, d\theta_{01}/dx, d\theta_{02}/dx), \tag{21}$$

where $(\Psi_h, \Phi_{1h}, \Phi_{2h})$ is the solution of homogeneous system obtained from Eqs. (17-19) by imposing $u_{f1} = 0$ and c is a constant. The values of u_{f1} and c can be found by substituting (21) into Eqs. (17)-(19) and (20). It leads to

$$c = -\{\Phi_{1h}/\theta_0^I\}|_{x=x_*}, \quad u_{f1} = -\lambda c.$$

Finally, the eigenvalue λ can be calculated by solving the homogeneous counterpart (imposing $u_{f1} = 0$) of Eqs. (17)-(19)with constraint (20) omitted without loss of generality. In what follows subindex "h" denoting the homogeneous solution will not be applied.

It should be noted that the steady-state solutions in the form of traveling waves are always invariant with respect to a shift $x \to x + const$. It leads to existence of the eigenvalue $\lambda = 0$ with the corresponding eigenfunction given by $(\Psi, \Phi_1, \Phi_2) = (dY_0/dx, d\theta_{10}/dx, d\theta_{20}/dx)$. The method applied in this study is able to calculate the eigenvalue with the largest real part, see [27]. Then, the eigenvalue $\lambda = 0$ can be obtained as a result (within numerical accuracy) in the case of a stable combustion wave.

6 Linear stability results

In order to compare the stability properties of the combustion wave in the composite sample with those in the pure energetic one we plot in Fig. 4 the growth rate λ_R calculated for $\xi = 0$ (the conductive core is absent) as a function of β for different values of the heat release parameter γ. In fact, these results presented here for the sake of completeness are equivalent to those for the stability of a planar flame front in an unbounded environment for $k = 0$, see [20], where k is the transverse wavenumber of perturbations. The critical values of the Zeldovich number β_c

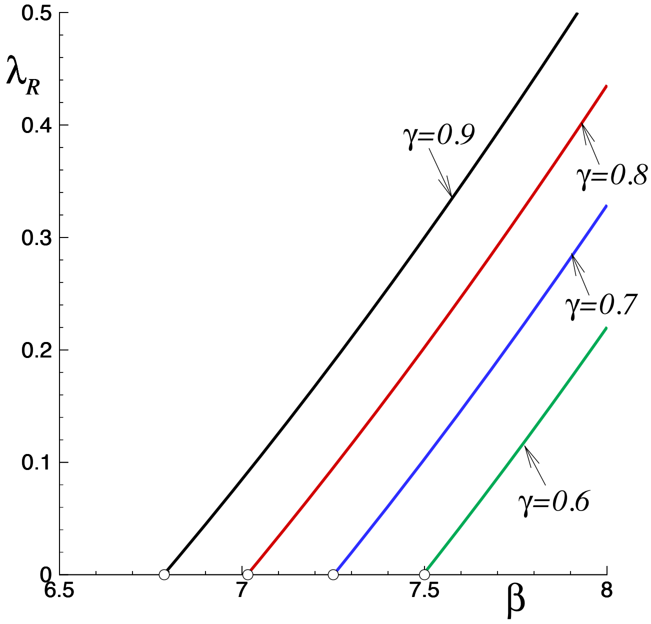

Figure 4: The growth rate λ_R plotted as a function of β for various γ corresponding to the pure energetic material case; the traveling wave solution becomes unstable for $\beta > \beta_c$ shown with a open circles.

above which the flame becomes unstable are indicated in Fig. 4 with open circles. In particular, the critical Zeldovich number for $\gamma = 0.7$ is $\beta_c \approx 7.25$.

Consider the case when the flame propagation in the pure energetic sample is stable taking $\beta = 7.2 < \beta_c$ for $\gamma = 0.7$. The dependencies of the growth rate λ_R and the frequency of oscillations on the parameter μ are plotted in Fig. 5 for various ξ. The left figure shows that with increasing values of ξ an interval of μ appears where λ_R comes to be positive. It is remarkable that the combustion wave recovers its stability for sufficiently small and sufficiently large values of μ. On the other hand, the parameters μ and ξ have little effect on the frequency of oscillations λ_I.

Figure 6 illustrates the case with $\beta = 8 > \beta_c$ when the combustion wave is already unstable in the pure energetic sample showing the dependence of the growth rate λ_R on the parameter μ for several values of ξ. All curves originate at $\mu = 0$ from the same point indicated with a dark circle corresponding to the growth rate of the (unstable) one-dimensional combustion wave in the pure energetic sample. One can see in Fig. 6 that λ_R initially increases with increasing

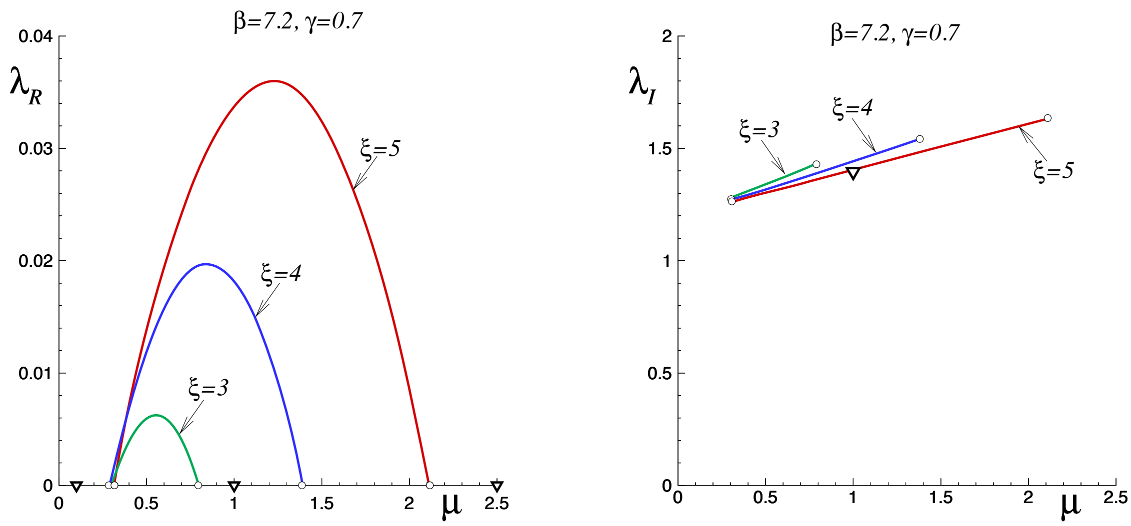

Figure 5: The growth rate λ_R (left) the frequency of oscillation λ_I (right) as a function of μ calculated for $\beta = 7.2, \gamma = 0.7$ and various ξ. The critical values of μ are indicated with open circles; open triangles in the left figure correspond to the numerical cases shown in Fig. 7 for $\xi = 5$; an open triangle in the right figure shows the frequency of oscillations computed from the direct numerical simulations for $\xi = 5$ and $\mu = 1$.

values of μ, peaks and thereafter decreases turning to be negative. The critical values of μ above which the flame propagation becomes stable ($\lambda_R < 0$) are marked with open circles.

7 Unsteady flame dynamics

In the present section the results of the linear stability analysis are contrasted with the nonlinear flame dynamics. The time-dependent problem given by Eqs. (6)-(7) and (11) was solved numerically. Consider first the case $\beta = 7.2$ for which the combustion wave is stable (the flame velocity is a constant in time) in the pure energetic sample. Figure 7 shows the time-histories of u_f calculated for $\xi = 5$ and three values of μ marked with triangles in Fig. 5. This plot demonstrates that for $\mu = 0.1$ and $\mu = 2.5$ the flame approaches after a transient stage of behavior a stable steady state. For $\mu = 1$, on the other hand, the solution evolves to a time-periodic state, with the flame velocity u_f oscillating with constant frequency and amplitude. Thus, for relatively low μ the flame propagation remains stable as well as in the pure energetic sample.

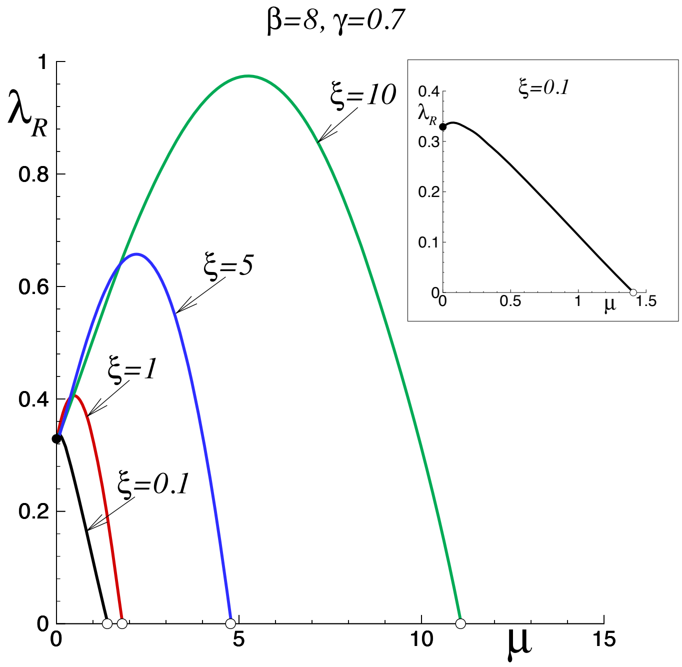

Figure 6: The growth rate λ_R as a function of μ for $\beta = 8$, $\gamma = 0.7$ and several values of ξ. The eigenvalue $\lambda_R = 0.3288$ corresponding to $\mu = 0$ (conductive core is negligible) is shown with a dark circle.

It becomes unstable undergoing periodic oscillations when μ is increased above the first critical value μ_*, but a further increase in μ above the second critical value μ_{**} leads eventually to re-stabilization of the flame propagation.

The direct numerical simulations themselves can be used to evaluate the flame stability properties, see [28]. We show in Fig. 5 (right) with an open triangle the frequency of oscillations λ_I obtained from the time-dependent code computed for $\mu = 1$ and $\xi = 5$. One can see a good fit of this result to the linear stability analysis.

The flame dynamics becomes much more complex for higher values of the Zeldovich number. Consider the case $\beta = 8$ and $\gamma = 0.7$ when the combustion wave is already unstable in the pure energetic sample. In Fig. 8 we show the time-history of u_f for various values of μ. All cases were calculated for $\xi = 5$ and the reference temperature was fixed at $\theta_* = 0.5$. One can see that with increasing values of μ the flame dynamics suffers important changes evolving from merely oscillatory, as shown by the $\mu = 0.1$ case, through the period-doubling route, the

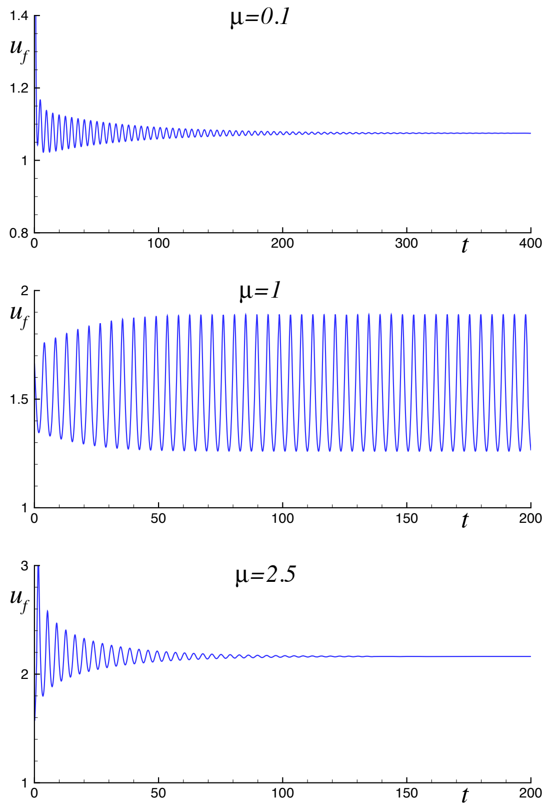

Figure 7: Time histories of the flame velocity calculated for $\beta = 7.2$, $\gamma = 0.7$, $\xi = 5$ and several values of μ corresponding open triangles in Fig. 5; the reference temperature is fixed at $\theta_* = 0.5$ for all cases.

cases $\mu = 1$ and 2.2, to the chaotic behavior illustrated with $\mu = 2.5$ and $\mu = 3$. It is notable that further increase in μ produces the inverse period doubling cascade illustrated with the $\mu = 4$ case, and, finally, leads to stabilization of the flame propagation shown for $\mu = 5$.

The chaotic flame dynamics found for $\mu = 3$ is compared with the simple oscillatory behavior observed for $\mu = 0.1$ in Fig. 9 where the dependence of the temperature maximum $\theta_{1\,max}$ is plotted versus the flame velocity u_f.

The simplest tool to illustrate variations in the flame dynamics is the first return map technics. Using the dependence of u_f as a function of time the series of the local maximum of the flame velocity are identified, $\{u_{f\,n},\ n = 1, 2, \dots\}$, where n is the maximum number. The dependence of $u_{f\,(n+1)}$ versus $u_{f\,n}$ is plotted in Fig. 10 for various μ. These pictures display the evolution of the flame dynamics with increasing values of μ.

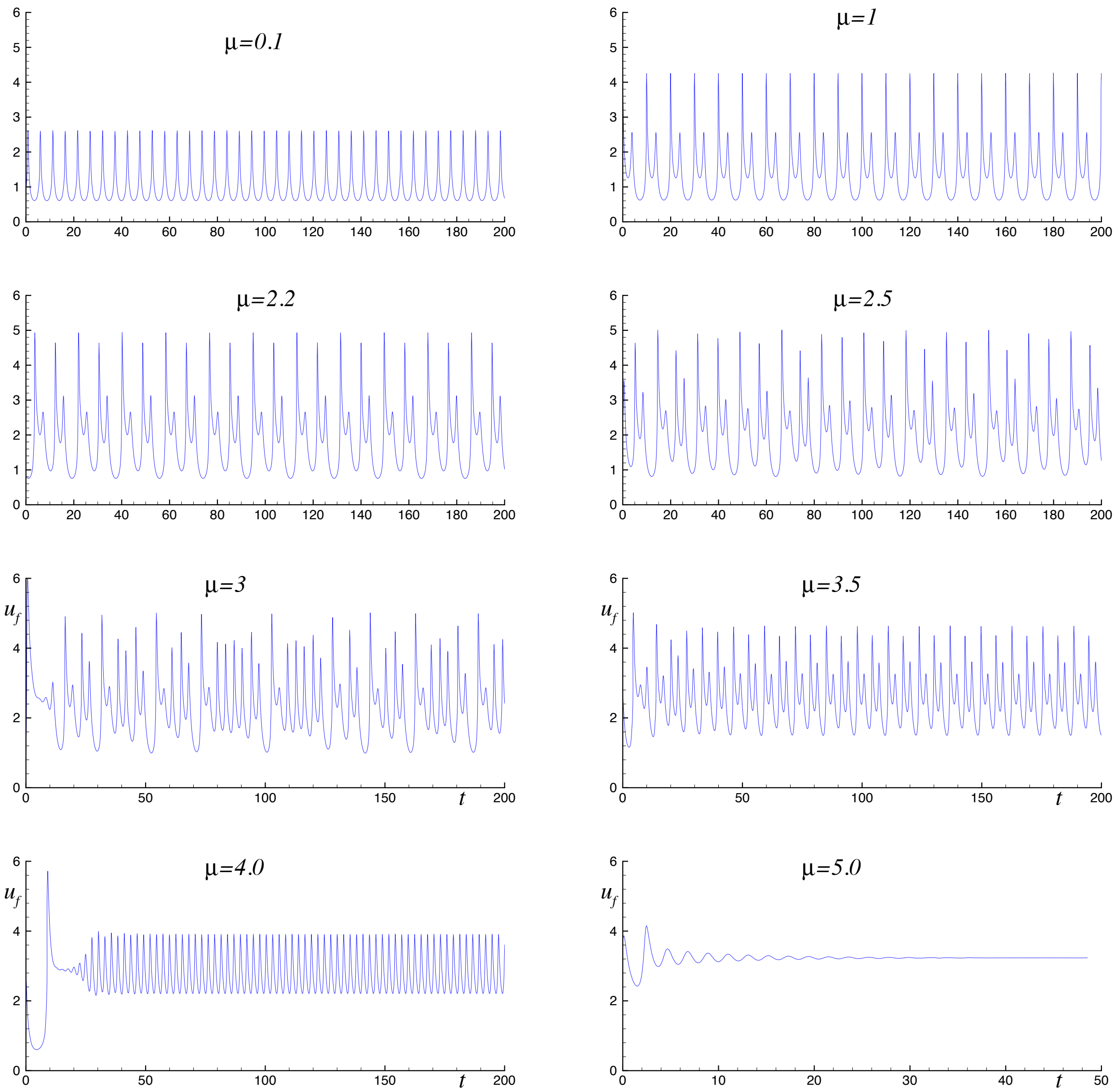

Figure 8: Time histories of the flame velocity calculated for $\beta = 8, \gamma = 0.7, \xi = 5$ and several values of μ; the reference temperature is fixed at $\theta_* = 0.5$ for all cases.

The case $\mu = 0.1$ illustrates a simple oscillatory behavior with the only maximum of u_f during the period: the first return map consists of a single point. The first return maps for $\mu = 1$ and $\mu = 2.2$ contain two and four points, respectively, indicating the typical period doubling cascade. The further increase in μ produces the first return map to be continuous evidencing the chaotic behavior of u_f on time. It is interesting to see in Fig. 10 that for $\mu = 2.5$ the first return

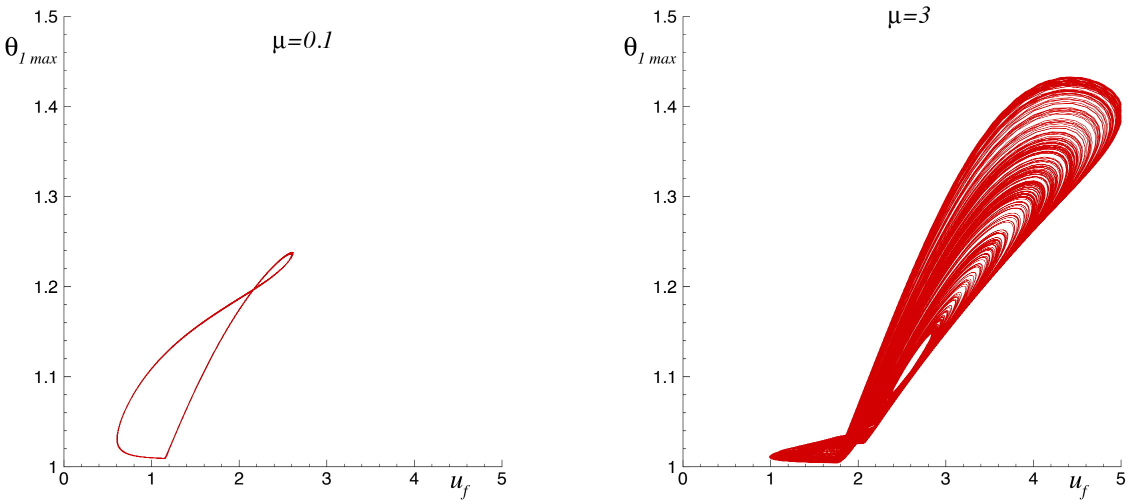

Figure 9: The dependence of θ_{1max} versus u_f for the mere oscillatory dynamics (left plot) and the chaotic regime (right plot).

map consists of various separated continuous parts which merge later for higher values of μ, as shown for $\mu = 3$. Thereafter, with further increase of μ, the first return map is split again into various parts, as shown for $\mu = 3.42$. Finally, the inverse doubling cascade are observed, as shown for $\mu = 3.5, 3.7$ and 4.

8 Lyapunov characteristic exponent

Evidently, the flame dynamics considered as a whole should be independent on the reference frame used to describe the process. In the present study we use the reference frame attached to a point with a fixed temperature, $\theta = \theta_*$. For the steady propagation the flame moves as a rigid structure and the (constant) flame velocity u_f is independent on θ_* due to invariance with respect to a shift along the direction of motion, $x \to x + const$. In the case of unsteady flame dynamics the flame does not move as a rigid structure, because each point of the flame moves with own velocity. Consequently, the specific form of u_f does depend on the choice of the reference temperature θ_*. In a certain sense the specific value of θ_* plays the role of an observable parameter determined by the choice an experimentalist.

Figure 11 shows the first return maps calculated for the same set of the physical parameters

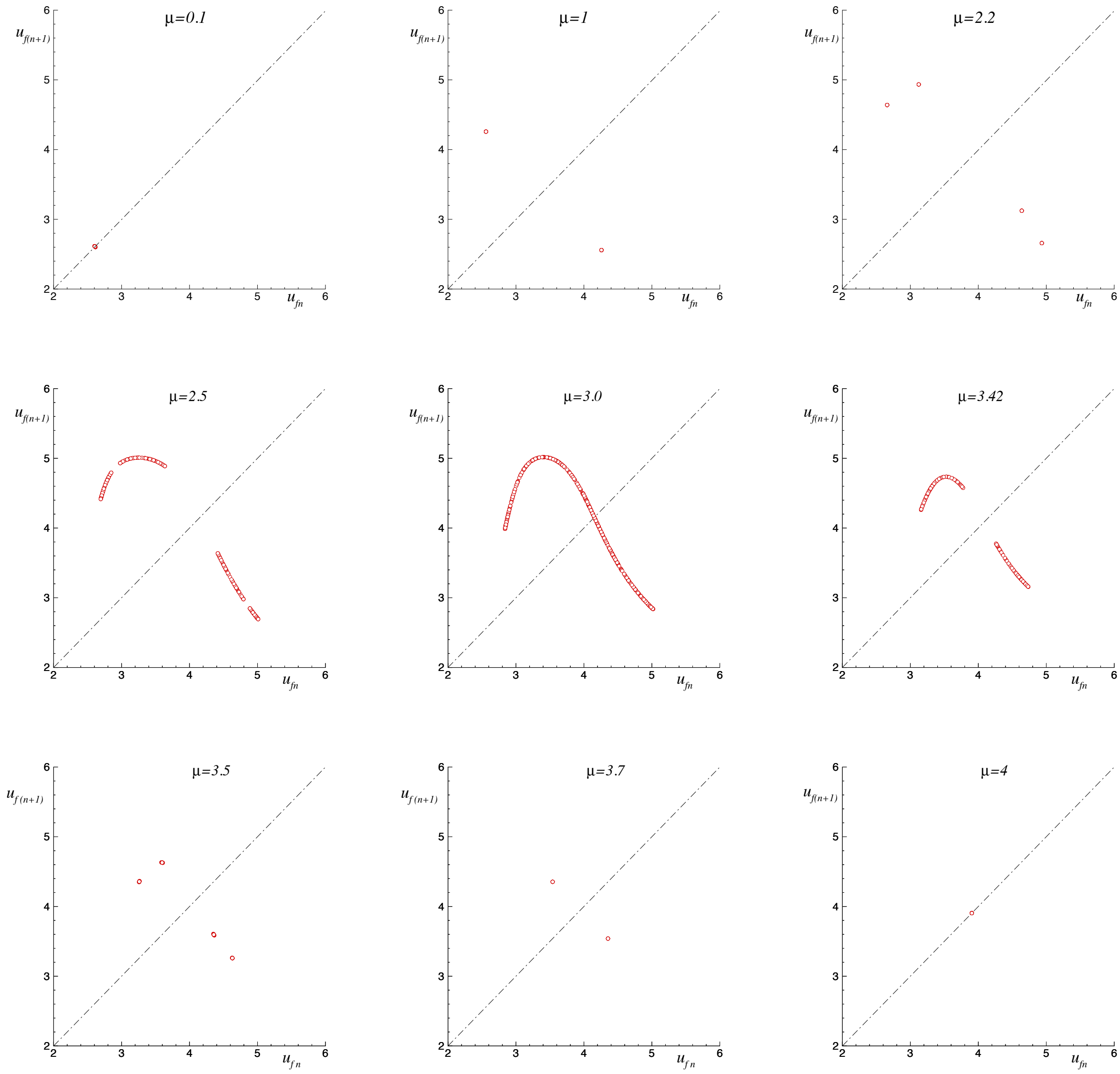

Figure 10: The first return maps of the relative maximum of u_f plotted for $\beta = 8$, $\gamma = 0.7$, $\xi = 5$ and various μ.

and different values of the reference temperature θ_* in the case of the chaotic flame dynamics. The figure shows that the maps are qualitatively similar, as one would expect, but the amplitude of chaotic oscillations is affected significantly by the choice of θ_*.

The level of randomness of time series can be characterized by the Lyapunov characteristic exponent [29]. In order that such calculations to be made the first return maps from Fig. 11 were approximated using tenth order interpolating polynomial. The Lyapunov exponent defined in

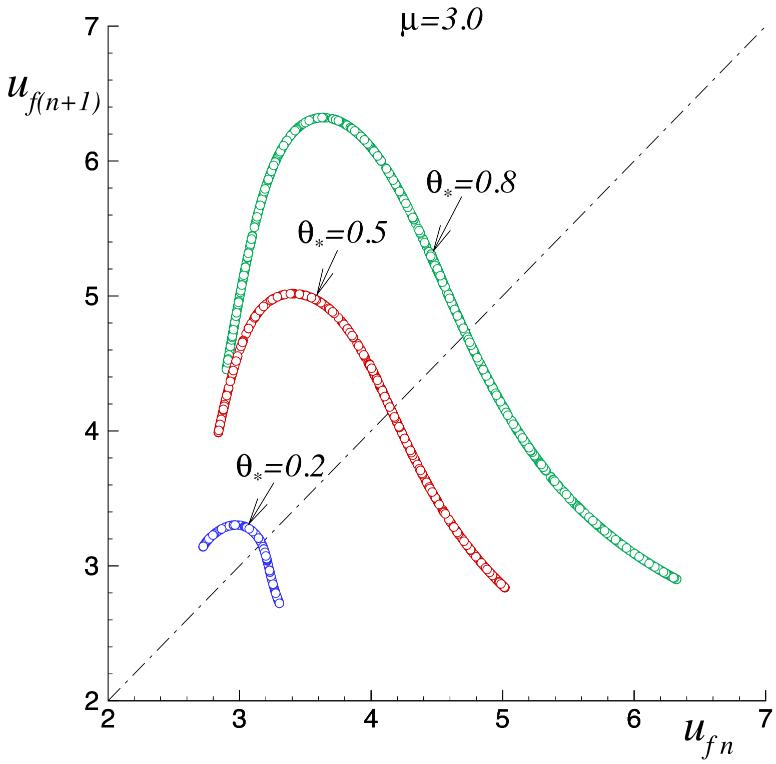

Figure 11: The first return maps of u_f calculated for $\beta = 8, \gamma = 0.7, \xi = 5, \mu = 3$ and different values of the reference temperature θ_*.

the ordinary way,

$$\lambda_L = \lim_{N\to\infty} \frac{1}{N} \ln \left| \prod_{i=1}^{N} f'(u_{f\,i}) \right|, \tag{22}$$

where $f(z)$ is the interpolating polynomial, was calculated for finite N. It was verified that for N above 10^4 the influence of the total number of iterations on λ_L becomes negligible. Figure 12 shows the variations of λ_L with θ_*. One can see that the choice of the reference temperature affects perceptibly the level of randomness of the stochastic dynamics.

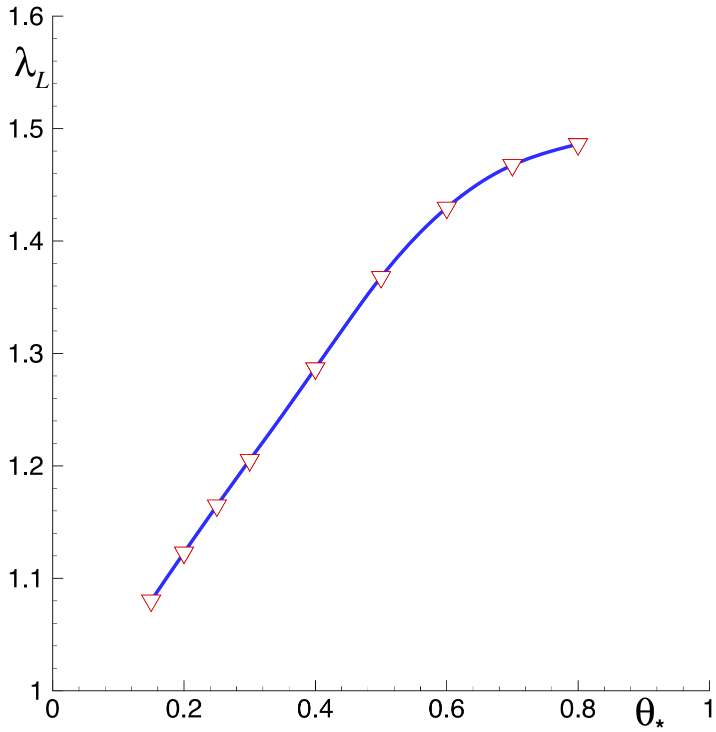

Figure 12: Lyapunov characteristic exponent computed computed using different reference temperature θ_*; for $\xi = 5, \beta = 8, \gamma = 0.7$ and $\mu = 3$.

9 Conclusions

The model describing the propagation of combustion waves in composite energetic material having a structure of the reactive shell-inert core type is derived and investigated for practically important case of large thermal conductivity and small cross sectional area of the inert core. This situation is encountered, for example, in the case of carbon nanotubes used as a thermal conducting element of the composite.

It is demonstrated that characteristics of flame propagation such as speed and the type of dynamical regime can be effectively controlled and manipulated, for fixed chemical properties, by varying the experimental parameters of the material i.e. the thickness of the fuel annulus deposited and the diameter of the heat conducting core. The different types of dynamical regimes include traveling, pulsating and chaotic waves. It is shown that the variation of the control parameter allow to modify the velocity of combustion wave propagation from the value corresponding to the adiabatic combustion wave in pure solid fuel to the values which are more then 5 times faster. Besides that the maximum temperature in the energetic annulus can be adjusted from the adiabatic flame temperature of pure solid fuel to the value exceeding it over 30 % and more. This can be very important and beneficial for combustion wave synthesis of solid materials and realization of the concept of chemical furnace.

Complex dynamics of flame propagation are investigated. It is demonstrated that the chaotic regime of combustion can be realized. The level of stochasticity of the process measured by the Lyapunov exponent is also shown to be controlled by the experimentally adjustable geometric parameters of the material. It is interesting to note that for such distributed active system as combustion wave in solid composite fuel the Lyapunov exponent depends on the choice of observable variables. This can be important for possible experimental diagnostics of chaotic flames.

From point of view of practical applications the emergence of transient and chaotic regimes with strong relaxation behavior, as demonstrated numerically in [15], can be undesirable due to effectiveness and safely issues. The former is due to the fact that the onset of oscillations may result in the incomplete conversion or even flame quenching. Whereas the latter may have implications to safety, since in the relaxation mode of oscillations there periodically appear bursts-like temperature peaks which are hard to predict and which may cause thermal runaways and local overheating. This motivates the study of complex dynamical regimes in such materials. In the nearest future we plan to undertake an experimental investigation of combustion dynamics of the shell-core energetic system made of thin metal wires and solid fuel. In such configuration the flame oscillations may be detected and analyzed with high-speed imaging and oscillations of luminosity.

Acknowledgements

VNK acknowledge the support of Spanish MEC under Project #ENE2015-65852-C2-2-R; VVG and RVF acknowledge the financial support from RFBF grant number 16-03-00758 and The Ministry of Education and Science of Russian Federation (grant 14.Y26.31.0003).

References

[1] A.F. Belyaev, L.D. Komkova, Dependence of burning velocity of thermites on pressure, Zh. Fiz. Khim 24 (1950) 1302-1311.

[2] L.B. Maksimov, Issledovanie pulsatsii svecheniya pri gorenii nitroglitserinovih porohov, Zh. Phys. Khim 37 (1963) 1129-1332.

[3] V.M. Shkiro, G.A. Nersisyan, Structure of fluctuations occurring in the burning of tantalum-carbon mixtures, Combusti. Explos. Shock Waves 14 (1978) 121-122.

[4] A.G. Merzhanov, A.K. Filonenko, I.P. Borovinskaya, New phenomena during combustion of condensed systems, Dokl. Akad. Nauk SSSR, Seriya Khimiya 208 (1973) 892-894.

[5] Yu.M. Maksimov, A.G. Merzhanov, A.T. Pak, M.N. Kuchkin, Unstable combustion modes of gasless systems, Combust. Explos. Shock Waves 17 (1981) 393-400.

[6] A.I. Volpert, V.A. Volpert, V.A. Volpert, Traveling wave solutions of parabolic systems, Vol. 140. American Mathematical Soc., 1994.

[7] A.G. Merzhanov, E.N. Rumanov, Physics of reaction waves, Rev. Modern Phys. 17 (1999) 1173-1211.

[8] A.S. Rogachev, A.S. Mukas'yan, Combustion Synthesis of Materials: Introduction to Structural Macrokinetics, Fizmatlit Moscow, 2012.

[9] K.G. Shkadinskii, B.I. Khaikin, A.G. Merzhanov, Propagation of a pulsating exothermic reaction front in the condensed phase, Combust. Explos. Shock Waves 7 (1971) 15-22.

[10] B.J. Matkowsky, G.I. Sivashinsky, Propagation of a pulsating reaction front in solid fuel combustion, SIAM J. Appl. Math. 35 (1978) 465-478.

[11] R.O. Weber, G.N. Mercer, H.S. Sidhu, B.F. Gray, Combustion waves for gases ($Le = 1$) and solids ($Le \to \infty$), Proc. R. Soc. Lond. A 453 (1997) 1105-1118.

[12] V.V. Gubernov, G.N. Mercer, H.S. Sidhu, R.O. Weber, Evans function stability of combustion waves, SIAM J. Appl. Math. 63 (2003) 1259-1275.

[13] G.I. Sivashinsky, On spinning propagation of combustion waves, SIAM J. Appl. Math. 40 (1981) 432-438.

[14] S.B. Margolis, B.J. Matkowsky, Nonlinear stability and bifurcation in the transition from laminar to turbulent flame propagation, Combust. Sci. Tech. 34 (1983) 44-77.

[15] A. Bayliss, B.J. Matkowsky, Two rounts to chaos in condensed phase combustion, SIAM J. Appl. Math 50 (1990) 437-459.

[16] A. Bayliss, B.J. Matkowsky, Interaction of counterpropagating hot spots in solid fuel combustion, Physica D: Nonlinear Phenomena, 128 (1999) 18-40.

[17] T.P. Ivleva, A.G. Merzhanov, Structure and variability of spinning reaction waves in three-dimensional excitable media, Physical Review E 64 (2001) 036218.

[18] A Bayliss, B.J Matkowsky, A.P Aldushin, Dynamics of hot spots in solid fuel combustion, Physica D: Nonlinear Phenomena 166 (2002) 104-130.

[19] T.P. Ivleva, A.G. Merzhanov, Three-dimensional modes of unsteady solid-flame combustion, Chaos 13 (2003) 80-86.

[20] V. N. Kurdyumov, C. Jiménez, V. V. Gubernov, A. V. Kolobov, Global stability analysis of gasless flames propagating in a cylindrical sample of energetic material: Influence of radiative heat-losses, Combust. Flame 162 (2015) 1996-2005.

[21] J.T. Abrahamson, N. Nair, M.S. Strano, Modelling the increase in anisotropic reaction rates in metal nanoparticle oxidation using carbon nanotubes as thermal conduits, Nanotechnology 19 (2008) 195701.

[22] W. Choi, S. Hong, J.T. Abrahamson, J.-H. Han, C. Song, N. Nair, S. Baik, M.S. Strano, Chemically driven carbon-nanotube-guided thermopower waves, Nat. Mater. 9 (2010) 423-429.

[23] K.Y. Lee, H. Hayoung, W. Choi, Advanced thermopower wave in novel ZnO nanostructures/fuel composite, ACS Appl. Mat. & Interfaces 6 (2014) 15575-15582.

[24] S. Jain, O. Yehia, L. Qiao, Flame speed enhancement of solid nitrocellulose monopropellant coupled with graphite at microscales, J. Appl. Phys. 119 (2016) 094904.

[25] V.V. Gubernov, V.N. Kurdyumov, A.V. Kolobov, Flame propagation in a composite solid energetic material, Combust. Flame 161 (2014) 2209-2214.

[26] V.V. Gubernov, V.N. Kurdyumov, A.V. Kolobov, Combustion waves in composite solid material of shell-core type, Combust. Theory Model 19 (2015) 435-450.

[27] V.N. Kurdyumov, Lewis number effect on the propagation of premixed flames in narrow adiabatic channels: Symmetric and non-symmetric flames and their linear stability analysis, Combust. Flame 158 (2011) 1307-1317.

[28] B. Denet, P. Haldenwang, A numerical study of premixed flames Darrieus-Landau instability', Comb. Sci. Tech., 104 (1995) 143-167.

[29] A.J. Lichtenberg, M.A. Lieberman, Regular and Chaotic Motion, Springer-Verlag 1983.